sustainability

MDPI

Article

A Novel Machine Learning-Based Approach for Fault Detection and Location in Low-Voltage DC Microgrids

Sirus Salehimehr, Seyed Mahdi Miraftabzadeh * and Morris Brenna

Department of Energy, Politecnico di Milano, 20156 Milano, Italy; sirus.salehimehr@mail.polimi.it (S.S.); morris.brenna@polimi.it (M.B.)

* Correspondence: seyedmahdi.miraftabzadeh@polimi.it

Abstract: DC microgrids have gained significant attention in recent years due to their potential to enhance energy efficiency, integrate renewable energy sources, and improve the resilience of power distribution systems. However, the reliable operation of DC microgrids relies on the early detection and location of faults to ensure an uninterrupted power supply. This paper aims to develop fast and reliable fault detection and location mechanisms for DC microgrids, thereby enhancing operational efficiency, minimizing environmental impact, and contributing to resource conservation and sustainability goals. The fault detection method is based on compressed sensing (CS) and Regression Tree (RT) techniques. Besides, an accurate fault location method using the feature matrix and long short-term memory (LSTM) model combination has been provided. To implement the proposed fault detection and location method, a DC microgrid equipped with photovoltaic (PV) panels, the vehicle-to-grid (V2G) charging station, and a hybrid energy storage system (ESS) are used. The simulation results represent the proposed methods' superiority over the recent studies. The fault occurrence in the studied DC microgrid is detected in 1 ms, and the proposed fault location method locates the fault with an accuracy of more than 93%. The presented techniques enhance DC microgrid reliability while conserving renewable resources, vital to promoting a greener and more sustainable power grid.

Keywords: DC microgrid protection; fault detection and location; regression tree; LSTM deep learning; renewable resources conservation

Citation: Salehimehr, S.; Miraftabzadeh, S.M.; Brenna, M. A Novel Machine Learning-Based Approach for Fault Detection and Location in Low-Voltage DC Microgrids. *Sustainability* **2024**, *16*, 2821. https://doi.org/10.3390/su16072821

Academic Editors: Chun-Lien Su, Te-Tien Ku and Chia-Hung Lin

Received: 30 January 2024
Revised: 12 March 2024
Accepted: 22 March 2024
Published: 28 March 2024

1. Introduction

The increasing growth of renewable energy sources (RESs), including solar photovoltaics (PV), fuel cells, energy storage systems, and also electric vehicles (EV) [1], has attracted more attention to DC microgrids as a practical solution for powering the DC loads in modern power systems [2]. The advancement of DC microgrids is progressing very fast due to their several advantages compared to the AC system. DC microgrids introduce an inherent decrease in AC systems' common problems, including synchronization, voltage quality, and frequency. Furthermore, the DC microgrid technology improves the power quality and reliability of the power system [3,4]. In a DC system, the reactive power drop and skin effects are eliminated, which results in more power flow compared to the AC system and a considerable reduction in power loss [5]. Due to the presence of renewable energy sources and DC loads in the system and the capability of DC microgrids to directly power them, the conversion stages are reduced, and the efficiency of DC microgrids is substantially increased [6]. Having all the referred advantages, the utilization of DC microgrids in power grids is still not as prevalent. One of the most important obstacles to widespread DC microgrids is the lack of comprehensive protection guidelines [7,8]. The challenging issues for DC microgrid protection include fault characteristics, fault type, fault location, and transient occurrence. In a DC microgrid, during a fault, fast discharging of the capacitors in the DC link results in increasing a significant multiplication of the

fault current amplitude [9,10]. The elevated current magnitude may seriously damage the equipment in the DC microgrid [11]. Accordingly, the utilization of very fast fault detection and precise fault location techniques is felt in these grids.

To safeguard DC microgrids from such faults, several approaches have been proposed. Due to its simplicity and cost-effectiveness, overcurrent protection is still one of the favorable protection techniques in DC microgrids. However, defining an accurate threshold value has always been a crucial issue for this method since the fault characteristics may vary by changing the DC microgrid topology [12,13]. The current derivative method is also proposed for fault detection in DC microgrids [14,15]. This technique uses the local measurements of the current signal derivatives to detect the fault. Based on this method, the fault is detected when the calculated current derivative is bigger than the pre-determined threshold value [16]. Using the local measurements, this method performs very fast and is a noise-resistant technique. Nevertheless, this method also suffers from determining a precise threshold value in different topologies of DC microgrids [17]. In some studies, the researchers have proposed differential protection as a fast and reliable protection for DC microgrids compared to overcurrent [18,19]. The advantage of using this method is its freedom from DG effects, fault current magnitude, and grid loading. However, this method requires a proper determination of threshold values to distinguish faults from transients occurring in microgrids [20]. For fault detection and location in DC systems, a method using traveling waves is proposed in [21], which this method shows a small error in this aim. Intelligent methods provide a swift and precise performance to detect faults in DC microgrids. However, in different grid types, they may illustrate different operations [22–24]. Regarding fault location, challenges arise due to the absence of frequency and phase data and the short line lengths within DC microgrids [20]. To address this, various methods have been developed for fault location determination. Utilizing online methodologies grounded in voltage and current fluctuations, the authors present a novel approach for fault location within a DC Ring Bus microgrid. The proposed method involves identifying fault occurrences by analyzing current oscillations following an incident and determining the faulted section through the examination of transient power variations during the initial cycle of the fault, as detailed in [25]. Furthermore, in [26], fault location within a Low-Voltage DC distribution network is achieved by leveraging DC magnitudes and directions, along with DC voltage levels. Proposed as an offline solution employing the Probe Power Unit (PPU) [5], a protective system has been introduced to both detect and locate faults. Another method for fault location in an LVDC microgrid is outlined in [27]. In contrast to the approach in [26], this method utilizes the attenuation constant of the damped probe current response. In [28], a fault location module is deployed at each end of a DC line, determining fault distance by sampling the discharge current through the line.

To overcome conventional fault detection and location problems, intelligent approaches like neural networks, fuzzy logic, and machine learning (ML) algorithms are employed [29,30]. Among the prediction techniques implemented to cope with power system challenges, ML approaches offer more accurate results. ML methods have been introduced as the primary tool for fault detection in distribution networks in [29]. This paper highlights methods including expert systems, Bayesian neural networks, LSTM networks, and support vector machines (SVM) as the most commonly utilized approaches for fault detection. However, they have more system requirements. In this regard, a technique based on the LSTM network is introduced in [31] for fault detection. This method uses the LSTM network to capture temporal features and SVM for classification. However, to implement this approach current, voltage, and active power have to be measured and used as input. Using the LSTM neural network, the authors have proposed a method for probabilistic sequence classification for fault detection in distribution grids in [32]. To detect faulty equipment in a microgrid, a convolutional neural network is proposed by [33]. However, this technique has a problem with protecting lines and loads. In [34], a combination of recurrent neural networks and a decision tree-based classifier is used to locate the

fault and detect disturbances in the system. Although this study shows an appropriate accuracy, it does not consider all potential components in the DC microgrid, such as the EV charging station. A fault detection and classification approach based on a decision tree is presented in [35] for microgrid protection. To extract features from raw data, discrete Fourier transform is utilized in this research. To detect faults in a microgrid, a method based on the combination of decision tree and wavelet transform is proposed in [36]. In [37], the authors have used a naive classifier, SVM, and an Extreme learning machine (ELM) to detect and classify the fault types in a microgrid. The data's feature is extracted using the Hilbert–Huang transform to implement the presented method. The authors in [38] have introduced an anomaly detection approach utilizing a deep neural network autoencoder, which effectively detects faults within the PV system. Considering the wind speed uncertainty, an ELM-based method is used in [39] to protect the microgrid. This study combines ELM and discrete wavelet transform to detect and classify the faults. A fault detection method based on a semi-supervised machine learning (SSML) model is introduced in [40]. In [41], an intelligent method for fault detection in a microgrid is proposed by a combination of wavelet transform and deep neural networks. The Markov model is another approach that is used by researchers in [42] to differentiate the fault condition from transients in a DC microgrid. The authors in [43,44] have used SVMs to identify fault conditions in DC systems. A variety of faults are taken into account and utilized to train the model parameters in [45], employing deep reinforcement learning as the foundation. A fault identification method for microgrids is developed using ML in [46]. In this research, initially, the voltage data are clustered using a modified K-means, and then association rules are extracted using the FP-growth algorithm. Finally, the fault identification model is trained using the mini-batch gradient descent (MBGD) algorithm based on ML principles.

According to the reviewed studies, it can be concluded that each method has its advantages and disadvantages. Based on the effectiveness of ML techniques in predictive tasks [47], this paper introduces a ML-based approach for fault detection and location in DC microgrids. The comparison of the proposed method with other existing studies in fault detection demonstrates the superiority of the presented technique given speed and accuracy in the detection of faults occurring in different locations in the microgrid. Furthermore, the proposed fault location method presents a high accuracy in locating the fault in the DC microgrid. In conclusion, the innovations presented in this article can be summarized as follows: (1) The combination of compressed sensing (CS) and regression tree (RT) for detecting various types of faults in DC microgrids. (2) Utilizing the feature matrix to train the LSTM model for fault location in DC microgrids. (3) Reduction in the required sampling rate compared to other signal processing methods. (4) Elimination of the threshold value due to preprocessing of training data. (5) Removal of telecommunication links and fault detection using sampled data from the main bus of the microgrid. (6) Considering the uncertainties of PVs and EVs and transient phenomena created by control systems.

This paper is structured into the following sections: the second part details the studied DC microgrid and provides the definitions and equations of the proposed fault detection and fault location techniques. In the third part, the proposed methods are evaluated, and the results are provided by figures and tables. Moving on to the fourth section, a comparison is conducted between the proposed fault detection method and recently published studies in this field. Finally, the fifth part concludes this paper.

2. Problem Formulation

The proposed method for fault detection in this paper takes advantage of the two techniques combination, CS and RT. The application of CS involves designing acquisition devices that utilize signal structure to lower the sampling rate, consequently reducing storage and digital signal processing (DSP) demands [48], while RT is a robust ML tool for building predictive models from data [49] On the other hand, to locate the fault in the DC microgrid, we have used the Long Short-Term Memory (LSTM) model. To obtain higher

accuracy in locating faults, a feature matrix from the current signal data has been used as input for this model. In the subsequent sections of this paper, the sample DC microgrid used to evaluate the proposed method has been reviewed. Then, proposed methods for fault detection and fault location in the DC microgrid are individually explained. To implement the proposed fault detection method, initially, a data set related to the normal and transient states of the DC microgrid is gathered by simulating these conditions. Afterward, CS is used to process this data set, and using the imaginary part of the signal the RT is trained. In this case, RT can predict the signal as long as it is in a normal or transient state; however, when a fault occurs in the DC microgrid, the difference between the predicted and the actual value of the signal will have a significant difference, and this feature can be used to detect the fault within the DC microgrid. The proposed fault detection approach is very fast and shows appropriate performance when transients occur in the system. In addition, this paper provides an accurate fault location method based on the feature matrix and LSTM model. In this step, the same DC microgrid is used and to generate data numerous pole-to-ground (PG) and pole-to-pole (PP) faults are applied to the main DC line. Therefore, current and voltage signals are measured at the IED location, and a feature matrix is extracted from these data. Afterward, the LSTM model is trained by the feature matrix and consequently, the proposed fault location method is evaluated by applying faults with random distances in the main DC line. The results present more than 93% accuracy for the fault locating with different fault resistances.

2.1. DC Microgrid Used for New Method Implementation

Figure 1 illustrates the structure of the DC microgrid being studied. The microgrid is equipped with different components including photovoltaic solar panels, an EV charging station, hybrid energy storage units (battery and flywheel), AC/DC and DC/DC converters, and various loads operating on both AC and DC power. Additionally, a modified five-layer control system, introduced by reference [50], has been used to stabilize the DC bus voltage. The DC bus voltage within this network is set to 600 V, while the AC voltage is defined at 380 V. Given the inherent unpredictability of generated power from PV and power consumption and delivery from EV, a hybrid energy storage system combining batteries and flywheel has been integrated to optimize energy management and distribution within the DC microgrid.

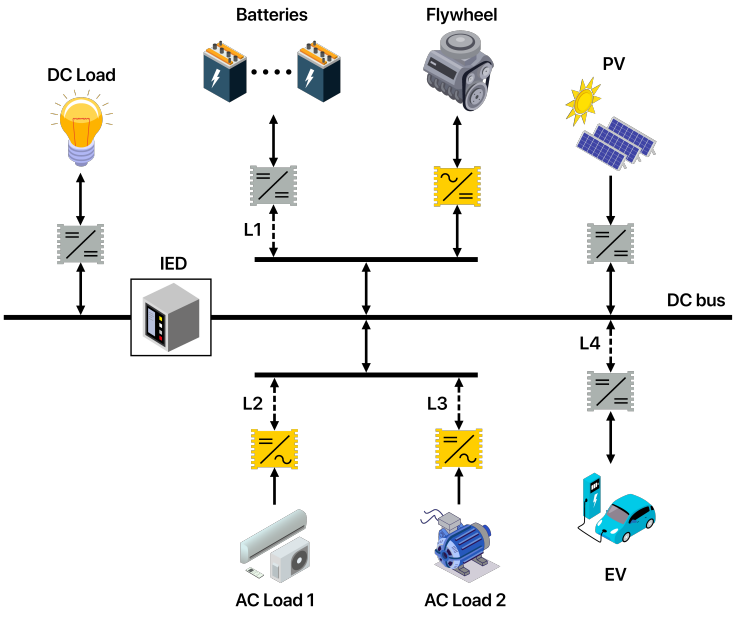

Figure 1. The DC microgrid used in this paper.

The PV model introduced in this paper is designed based on the model described in reference [50]. Key parameters of the PV cell, such as short-circuit current (I_{sc}), open-circuit voltage (U_{oc}), maximum power voltage (U_m), and current (I_m), are typically provided by the manufacturer. These parameters are determined under standard conditions with a temperature of $T_{ref} = 25$ °C, solar irradiance of $S_{ref} = 1000$ W/m^2, and spectrum AM1.5G.

In the EV model, the nominal voltage for the battery is 360 V, the rated capacity is 100 Ah, the initial state-of-charge is 70%, and the battery has a response time of 10 ms. The DC/DC EV converter also includes two IGBT/Diodes and an inductor as the filter.

Within this DC microgrid, we have incorporated two AC loads and one DC load, in which individual loads have their own distinct electrical parameters. The three-phase AC loads are resistive and work at the determined voltage level. The microgrid being examined is a two-wire DC system, comprising four lines. Each line has a cross-sectional area of 240 mm^2 and employs aluminum cables with PVC type A insulation and ST-1 PVC sheathing. The specific details about the microgrid are presented in Table 1.

Table 1. DC microgrid parameters [51].

	Parameter	Value
1	DC bus voltage	600 V
2	AC voltage	380 V
3	Bat.	LifePO4, 360 V, 100 Ah
4	PV Power	20 kW
5	Charg & disch. of EV	15 A & 10 A
6	AC loads	5 kW
7	DC load	5 kW
8	Flywheel	10 kW, 10,000/5000 r/min
9	Cables diameter	240 mm^2
10	Cables resistance	0.125 Ω/km
11	Cables Inductance	0.232 Ω/km
12	Cables lengths	1 km

2.2. Fault Detection Method

In this section, we introduce our novel approach for fault detection, harnessing the combined power of CS and RT. CS offers an efficient data representation method, while RT is a powerful tool for modeling complex data relationships. Sampling the signal using CS and utilizing the RT for prediction, the proposed method provides a robust and accurate fault detection system.

2.2.1. Compressed Sensing Theory

Following the conventional signal processing technique, the introduction of CS created significant progress within signal processing methods [52,53]. CS typically finds application in the acquisition of signals that have either sparsity or compressibility. We can determine a signal sparse/compressible in both original form or in transform domains such as Fourier transform, wavelet transform, and cosine transform.

CS operates based on recording fewer non-adaptive random measurements. Mathematically, CS can be formulated as follows: Let x be the original n-dimensional signal vector that we want to recover, and let y be the m-dimensional measurement vector obtained by multiplying the signal vector with the measurement matrix ϕ [54]:

$$y = \phi x \tag{1}$$

In this equation, the input signal $x \in \mathbb{R}^n$ (or we can say $x \in \mathbb{C}^n$) has a length of n. Sensing matrix $\phi \in \mathbb{R}^{m \times n}$ (can also be shown as $\phi \in \mathbb{C}^{m \times n}$) is typically a random or structured $m \times n$ matrix representing the measurements taken from the signal. Each row of ϕ corresponds to a measurement or sample of the signal. Finally, the measurement vector is shown by y (y $\in \mathbb{R}^m$ or $y \in \mathbb{C}^m$) having a length of m that here y represents

the measurement vector obtained by sampling the signal x using a sensing matrix ϕ. To generate the compressive measurements, the random measurement matrix and the input signal should be multiplied together. Accordingly, the number of taken measurements is significantly lower than the input signal length ($m \ll n$).

Here, the measurement random matrix ϕ is decomposed into two matrices H and P (2):

$$\phi = HP \tag{2}$$

where H is a matrix that defines the relationship between the original signal x and the measurements y. It essentially maps the original signal to the measurement space. P is a permutation matrix that rearranges or selects specific elements from the original signal vector x. The number of required samples for measurement is defined by the total number of samples in each of the rows in H; the ratio here is $R = [n/m]$. Here n represents the dimensionality of the signal being measured, and m shows the number of measurements or samples needed to accurately recover the signal. In the following, (3) and (4) represent the P and H matrices.

$$P = \begin{bmatrix} P_1 & & \\ & \dots & \\ & & P_n \end{bmatrix} \tag{3}$$

$$PH = \begin{bmatrix} 111\dots & & \\ & 111\dots & \\ & & 111\dots \end{bmatrix} \tag{4}$$

In addition, we can calculate $\bar{x}$ as:

$$\bar{x} = Px \tag{5}$$

where $\bar{x}$ represents the permuted or selected version of the original signal x. Therefore, we can rewrite (5) as the following:

$$y = H\bar{x} \tag{6}$$

Finally, in this equation, y represents the measurement vector obtained by linearly mapping the original signal x using the matrix H.

2.2.2. Regression Tree

Recent advancements in ML techniques have garnered attention to cope with the challenges confronting modern power systems [55]. The RT is known as a powerful ML tool used for decision-making and predictive modeling. It belongs to the family of decision trees and is specifically designed to solve regression problems, where the goal is to predict a continuous numeric value according to input characteristics. In this case, prediction errors are usually quantified by measuring the squared difference between the observed values and their related predictions [49]. Given the similarity between the RT and the classification tree, this section will commence with an expression of the classification tree, followed by a comprehensive examination of the RT.

In the context of a classification problem, we are presented with a training sample comprising n observations of a class variable denoted as Y, which assumes values $1, 2, \dots, k$, alongside p predictor variables, $X_1, X_2, \dots, X_p$. The primary objective is to establish a predictive model for estimating the values of Y based on new sets of X values. In principle, the solution involves partitioning the X space into K distinct sets—namely, $A_1, A_2, \dots, A_k$—such that the predicted value of Y corresponds to j if X falls within Aj, where j ranges from 1 to k. When the X variables assume ordered values, there are two well-established approaches, namely, linear discriminant analysis and nearest-neighbor classification [56]. These methodologies generate sets Aj characterized by piecewise linear and nonlinear boundaries, respectively.

The classification tree approaches employ a recursive partitioning approach to create rectangular sets Aj by sequentially dividing the dataset, focusing on one X variable at a time. This strategy results in sets that are inherently easier to interpret. A noteworthy advantage of the decision tree structure is its versatility in handling any number of variables, whereas the visualization on the left panel is inherently limited to a maximum of two variables.

A RT shares similarities with a classification tree, but it diverges in that the dependent variable Y takes ordered values, and each node employs a regression model to predict $Y's$ values [57].

As explained before, when the output variable is in nature qualitative, the classification tree is used. Conversely, an RT is considered when the data are quantitative. Accordingly, RT is of interest to this paper since our detection method deals with a quantitative issue. RT is a powerful technique for prediction and is constructed through a recursive process of dividing a dataset and fitting a simple model for each segment of the data [49]. The RT method is defined as a non-parameter algorithm and is known as an automatic classifier. Considering a learning sample having n cases that have the variables x and y $((x_1, y_1), (x_2, y_2), \ldots (x_n, y_n))$, an RT creates a classifier structured as a binary tree. In this definition, x_t represents the tth independent variable taking an m-dimensional vector form, while y_t corresponds to the response variable having a numerical value. In such RTs, the tree is built through iterative splits of subsets into a pair of descendant subsets based on sample input variables. Each split involves a question about the input variables, with "yes" and "no" responses guiding the creation of left and right descendant subsets, respectively [58].

2.2.3. Proposed Fault Detection Algorithm

The initial step to implement the proposed method in this paper is the precise sampling of the current signal within various grid conditions. These measurements are gathered at the Intelligent Electronic Device (IED) location. By simulating a wide range of transient and steady-state scenarios using the MATLAB/Simulink (version R2023a-academic use) environment, a diverse dataset is generated through sampling of the current signal. This comprehensive dataset mirrors the DC microgrid's behavior under different operational conditions, making it a valuable resource for fault detection. The current signal waveform in normal operation, transient, and the faulty condition of the system is demonstrated in Figures 2 and 3. According to the depicted waveform, for 2.2 s the DC microgrid is in normal operation. At exactly 2.2 s, a transient occurs due to the PV output change, and as shown in Figure 3, at the time of 2.5 s a PG fault occurs in the main DC line.

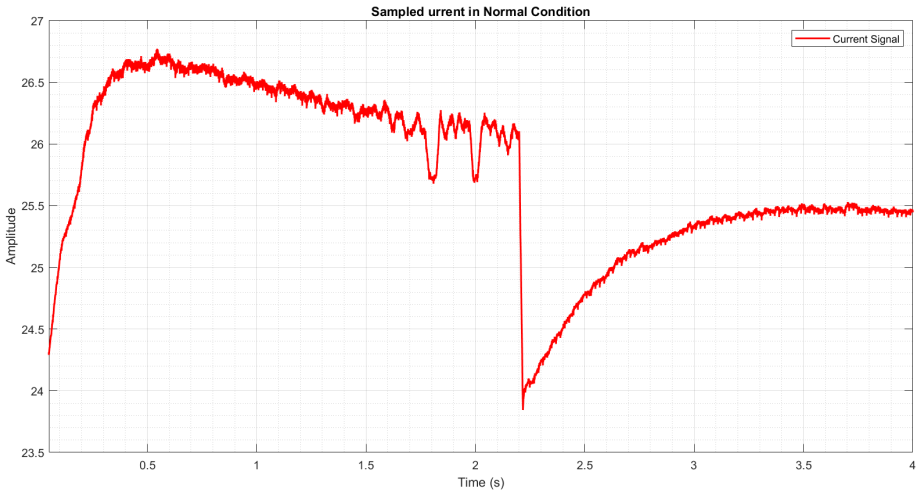

Figure 2. Current signal during normal operation and transient of the DC microgrid.

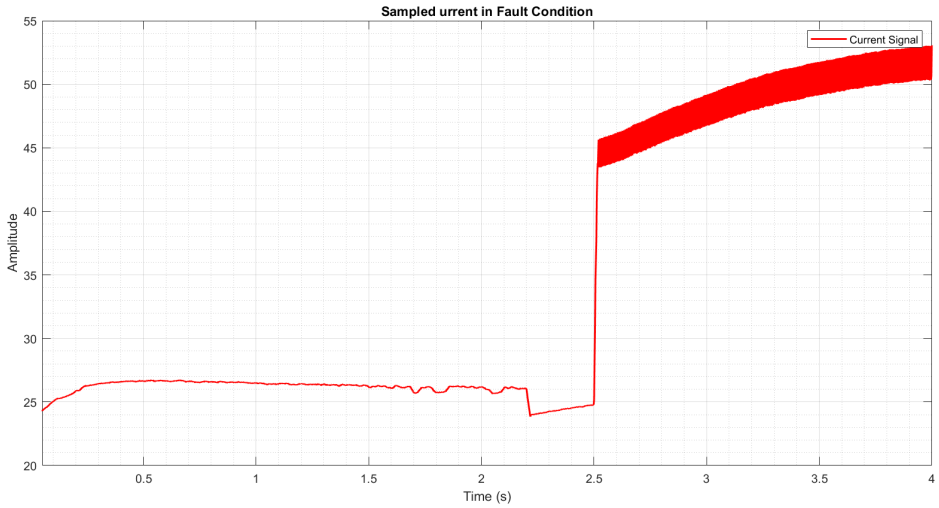

Figure 3. Current signal during normal operation, transient, and the faulty condition of the DC microgrid.

Subsequently, we employ CS to process this dataset. CS extracts the data of real and imaginary measurements. In the next stage, we undertake an offline procedure to train the RT using the output data derived from the CS. The trained RT is depicted in Figure A1 (Appendix A). This training phase equips our fault detection algorithm with the capability to effectively differentiate between normal operating conditions and anomalies. A visual representation of this detection algorithm is presented in Figure 4, enabling continuous monitoring and assessment of the DC microgrid's condition.

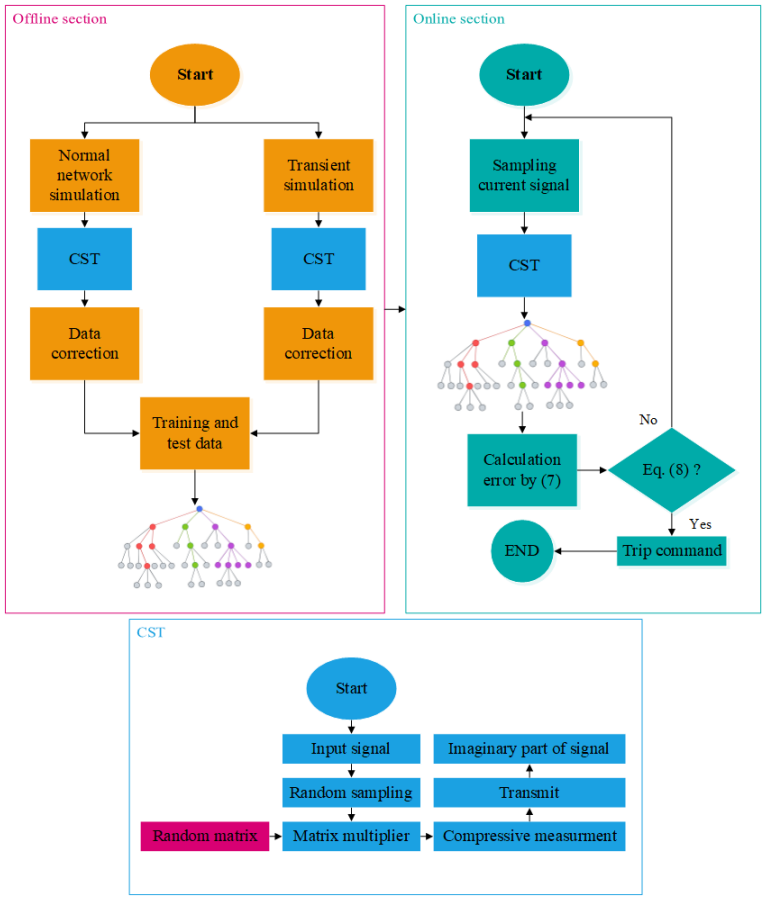

Figure 4. The algorithm of the proposed fault detection method.

Let us consider the algorithm in two parts; the offline part is related to RT training. On the other hand, the online part is related to the performance of the algorithm and checking if there is any fault occurrence in the grid.

In fact, we have trained the RT utilizing the data resulting from the imaginary part of the current signal, in which the signal is processed by CS. Since the RT is trained using DC microgrid normal conditions data, the difference between the actual and the predicted imaginary value of the current signal by RT will be zero for normal conditions of the grid. This statement can be explained by (7).

$$E = [\text{actual}_{Im} - \text{predicted}_{Im}] \tag{7}$$

where E is the representative of the absolute value of the error (difference between actual and predicted value), and Im refers to the imaginary part of the current signal. Accordingly, by defining the condition demonstrated in (8), the algorithm can decide how to perform for the various disturbances of the grid.

$$\text{If } E > 0, \text{ then (fault condition)} \tag{8}$$

According to Figure 4 and considering (8), if the difference between the actual and predicted value is zero, the occurred disturbance in the grid is a steady state or transient state and the algorithm should block the protection system operation. On the other hand, when the error value is greater than zero, the fault has occurred in the DC microgrid, and the trip command must be issued.

2.3. Fault Location

The previous section provided a fault detection algorithm in DC microgrids based on the CS signal processing technique and RT algorithm. However, in a DC microgrid, fault detection by itself is not enough to advance reliability, and the location of the fault should also be accurately determined. Moving forward, a robust technique for fault location in DC microgrids is developed by the implementation of the feature matrix and LSTM method. This approach harnesses the power of feature matrix and LSTM networks to enhance pinpointing the precise location of faults within the DC microgrid.

2.3.1. Feature Matrix

Since signals typically consist of complex data with high dimensions, they are not suitable for training intelligent techniques. For this reason, it is necessary to convert the signals into a straightforward and practical representation for intelligent models. Feature extraction from the signal enables intelligent algorithms to learn patterns, predict, and perform various data analysis tasks. Accordingly, in this article, the feature matrix extraction method presented in [59] is used to extract features from the current signal. This feature matrix includes features such as *Mean*, *RMS*, *Difference*, and *Maximum* value of the signal data. *Mean*, *RMS*, *Difference*, and *Maximum* value are major metrics used in feature extraction. Among these metrics, *Mean* represents the average value of a set of numbers. In error calculation, the *Mean* error indicates the average disparity between the predicted and the actual values over all data points in the dataset and provides an overall examination of the model's bias. The *RMS* is a statistical estimate computed by taking the square root of the average of the data set. The *Difference* measures the differences between individual values. The *Maximum* value within a feature matrix denotes the highest value existing in the dataset. To calculate these metrics, Equations (9)–(12) are used.

$$Mean = \frac{abs(IF)}{length(IF)} \tag{9}$$

$$RMS = \sqrt{\sum_{i=n}^{N} \frac{IF^2}{N}} \tag{10}$$

$$Difference = \sum_{i=n}^{N} (IF(i) - IF(i-1)) \tag{11}$$

$$Max = max(IF) \tag{12}$$

To create the feature matrix, numerous simulations are conducted at various intervals along the line, with each simulation representing a one percent increment of the line's length. In fact, these distances represent the fault impedance, and accordingly, the fault characteristics will be different for each distance. In these simulations, the fault time characteristics are taken into account to create the feature matrix. Consequently, the final form of the feature matrix is obtained by Equation (13). This matrix will be used to train the proposed LSTM model.

$$Feature\ Matrix = \begin{bmatrix} Mean \\ RMS \\ Diff \\ Max \end{bmatrix} \tag{13}$$

2.3.2. LSTM Model

The LSTM model is a type of Recurrent Neural Network (RNN) that resolves the challenges in traditional RNN models [60]. In this paper, the LSTM model has been used to implement the proposed method for fault location having input from the feature matrix. Figure 5 depicts the overview of the LSTM model.

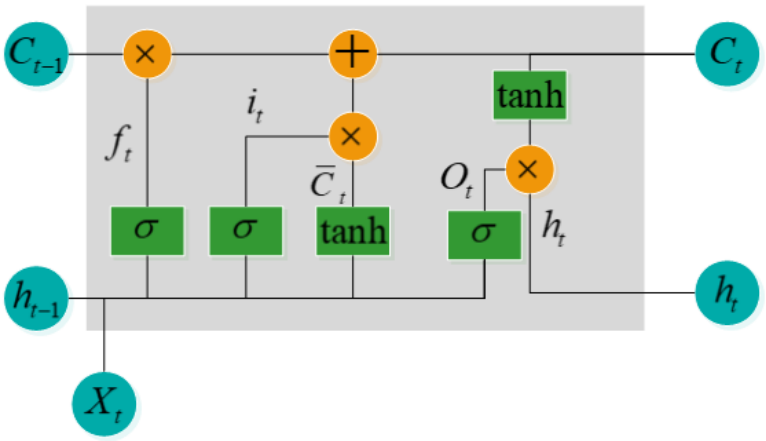

Figure 5. The structure of LSTM model.

The fundamental principle of the LSTM network is the introduction of several key components known as gates (forget gate, input gate, update gate, and output gate). The relationships governing these gates and memory units are determined based on the following equations [61,62].

The forget gate decides which information from the previous cell state to discard. Mathematically, it can be represented as:

$$f_t = \sigma(W_f \cdot [h_{t-1}, x_t] + b_f) \tag{14}$$

where σ represents the sigmoid activation function, W_f and b_f are the weight matrix and bias vector related to the forget gate, and h_{t-1}, x_t describes the sequence of the previous hidden state and the current input.

The input gate operation can be expressed mathematically as below:

$$i_t = \sigma(W_i \cdot [h_{t-1}, x_t] + b_i) \tag{15}$$

In addition, a candidate update vector is computed using the same input and is subsequently modified as follows:

$$\tilde{C}_t = \tanh(W_c \cdot [h_{t-1}, x_t] + b_c) \tag{16}$$

where W_i, W_c, b_i, and b_c are the weight matrices and bias vectors specific to the input gate and candidate update, respectively, and tanh shows the activation function.

The update gate determines the proportion of new candidate values to replace old cell state values. Mathematically, it can be expressed as:

$$C_t = f_t \odot C_{t-1} + i_t \odot \tilde{C}_t \tag{17}$$

In this equation, the previous cell state is shown by C_{t-1} and i_t and $\tilde{C}_t$ determines the new values.

Finally, the output gate controls which section of the current cell state has to be exposed or moved on to the output. The operation of the output gate can be expressed by the following equations.

$$o_t = \sigma(W_o \cdot [h_{t-1}, x_t] + b_o) \tag{18}$$

$$h_t = o_t \cdot \tanh(C_t) \tag{19}$$

In these equations, o_t represents the output gate activation vector, and h_t is the next hidden state. The tanh function is also applied to the updated cell state for the generation of a new hidden state.

2.3.3. Proposed Fault Location Algorithm

To implement the fault location algorithm, at first, the PG and PP faults are applied to the main DC line at different distances. The intervals for applying the fault are divided by one percentage of the line. Afterward, the voltage and currents at the line are measured at the IED location, and the data are used to create the feature matrix and then train the LSTM model. To have a better overview of the proposed algorithm, let us consider Figure 6.

As can be seen from this figure, in an offline procedure, the current and voltage signals are continuously sampled. When a fault occurs, the process is started by creating the feature matrix. When the matrices *Mean*, *RMS*, $Difference$, and *Maximum* value are calculated, the feature matrix is obtained using these key matrices. Consequently, the feature matrix extracted from every window signal of the voltage and current signals is saved in a dataset. In the next step, the LSTM model is trained utilizing this dataset. Now, the trained LSTM model needs to be evaluated to ensure its accuracy in fault location. MAE (Mean Absolute Error), MSE (Mean Squared Error), and $RMSE$ (Root Mean Squared Error) are commonly used metrics for evaluating the accuracy of LSTM models in prediction tasks. Based on the equations, MAE measures the average absolute difference between predicted and actual values, MSE measures the average squared difference between predicted and actual values, and $RMSE$ is the square root of MSE and provides a measure of the typical error magnitude. To do this, the Equations (20)–(22) are considered, and the results show the model accuracy [60].

$$MSE = \frac{1}{N} \times \sum_{t=1}^{N} (L_t^{Measured} - L_t^{Forcast})^2 \tag{20}$$

$$RMSE = \sqrt{\frac{1}{N} \sum_{t=1}^{N} (L_t^{Measured} - L_t^{Forcast})^2} \tag{21}$$

$$MAE = \frac{1}{N} \sum_{t=1}^{N} |L_t^{Measured} - L_t^{Forcast}| \tag{22}$$

Finally, achieving the accuracy of the LSTM model, the precise location of the fault can be ensured. Therefore, in the online procedure, the algorithm starts gathering data by the occurrence of a fault, and utilizing the trained LSTM model faults in different distances of the line can be located. According to this figure, when the fault occurs on the main DC line, the algorithm is activated, and using the data obtained from the current and voltage signals at the IED location locates the fault with high accuracy and in a short time.

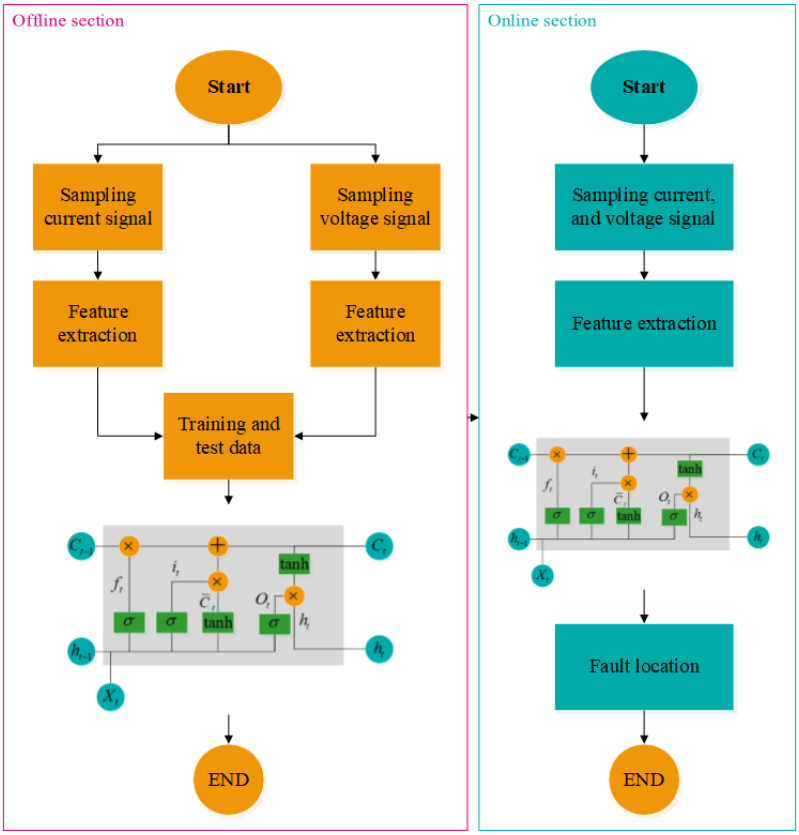

Figure 6. The process of LSTM model training and evaluation.

3. Simulation Results

In this section of the paper, we present the observational results that validate the efficacy of our innovative fault detection and location methods for DC microgrids.

3.1. Fault Detection Results

In the context of assessing the efficacy of the proposed fault detection method within the DC microgrid, various arrays of potential scenarios were evaluated. This examination encompassed pole-to-ground (PG)and pole-to-pole (PP) faults on the main line and the faults occurring within the microgrid's distributed energy sources. The case studies examine various fault impedances present in different sections of the DC microgrid, which are commonly investigated scenarios in recent studies [51].

3.1.1. Case 1: Fault in the Main DC Line

To evaluate the performance of the proposed method for PG fault conditions, a fault with different resistances of 1.5 Ω, 2.5 Ω, and 5 Ω is applied on the main line on the studied DC microgrid shown in Figure 1. The fault is applied at the time of 2.5 s. The results for the PG fault on the main DC line are depicted in Figure 7. As can be seen, during the steady state or transients (at the time of 2.2 s) the difference between the actual value and the predicted value is zero. However, when the fault occurs, the error value jumps to a higher value and the algorithm detects the fault in 1 ms.

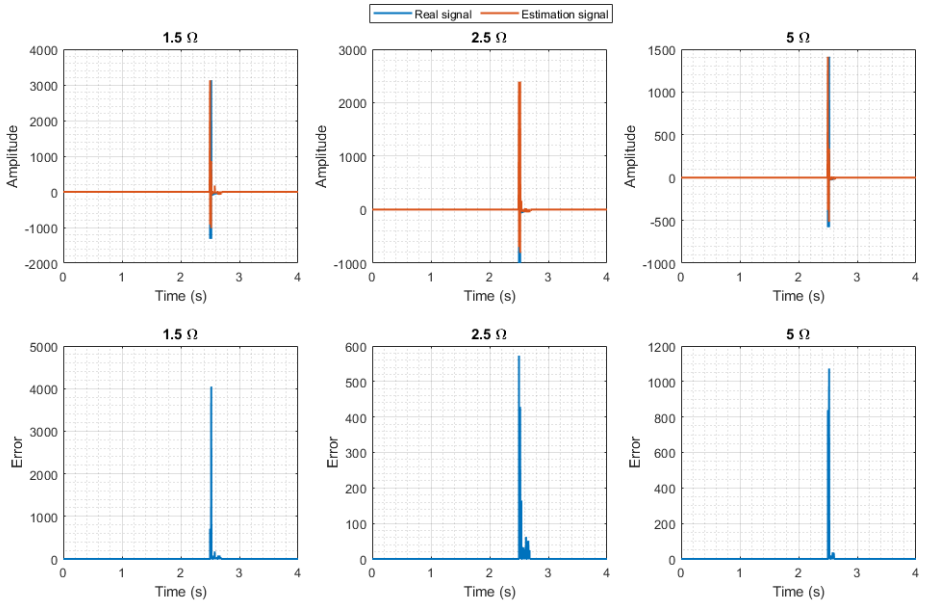

Figure 7. The proposed method performance for the PG fault in the main line.

To evaluate the performance of the proposed method when occurring PP fault, a PP fault with the same range of resistances, as the previous case, is applied in the main DC line and the results can be seen in the figure below (Figure 8).

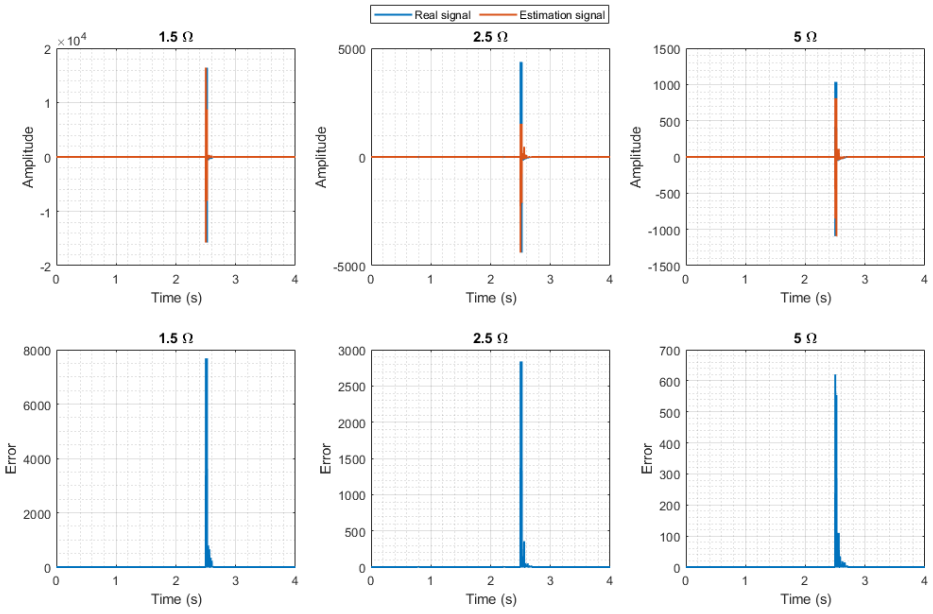

Figure 8. The proposed method performance for the PP fault in the main line.

3.1.2. Case 2: Fault in PV

To examine the operation of the proposed fault detection method when a PG fault occurs in the PV, a PG fault is applied on the PV output and before the DC/DC boost converter. The fault resistance and the fault time are the same as previous case. According to the simulation result for this case, we can see that the proposed method precisely detects the fault in 1 ms (Figure 9).

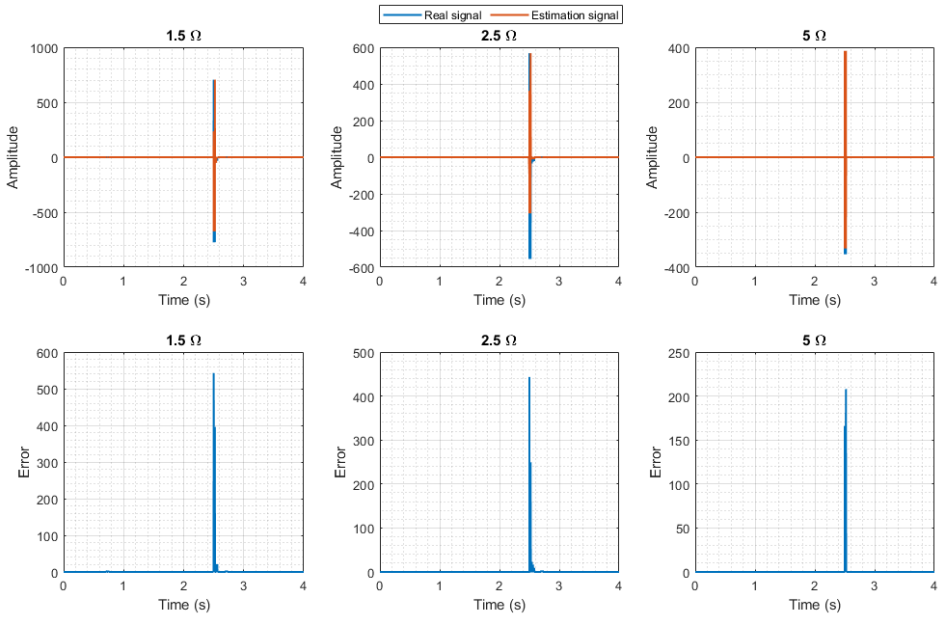

Figure 9. The proposed method performance for the PG fault in the PV.

The performance of the proposed method for the PP fault in the PV is evaluated by applying a PP fault in the same location with the same characteristics and the results are shown in Figure 10.

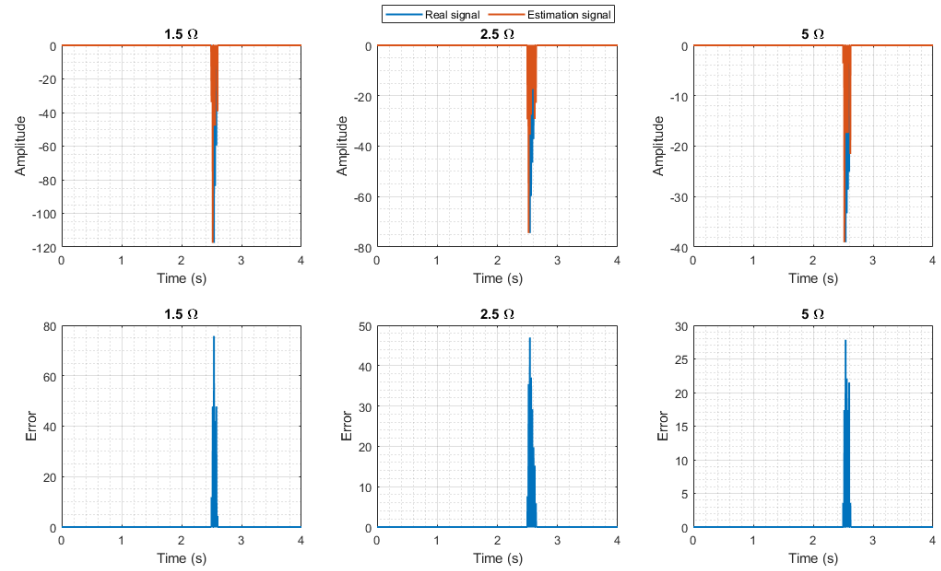

Figure 10. The proposed method performance for the PP fault in the PV.

3.1.3. Case 3: Fault in EV

For the examination of the presented fault detection method performance when a PG fault occurs in the EV system, a fault is placed in the EV system. The fault time is similarly t = 2.5 s, and the fault resistances are similar to previous cases. Based on the results shown in Figure 11, it can be seen that the proposed method operates accurately for the PG fault in this case and detects the fault in 1 ms.

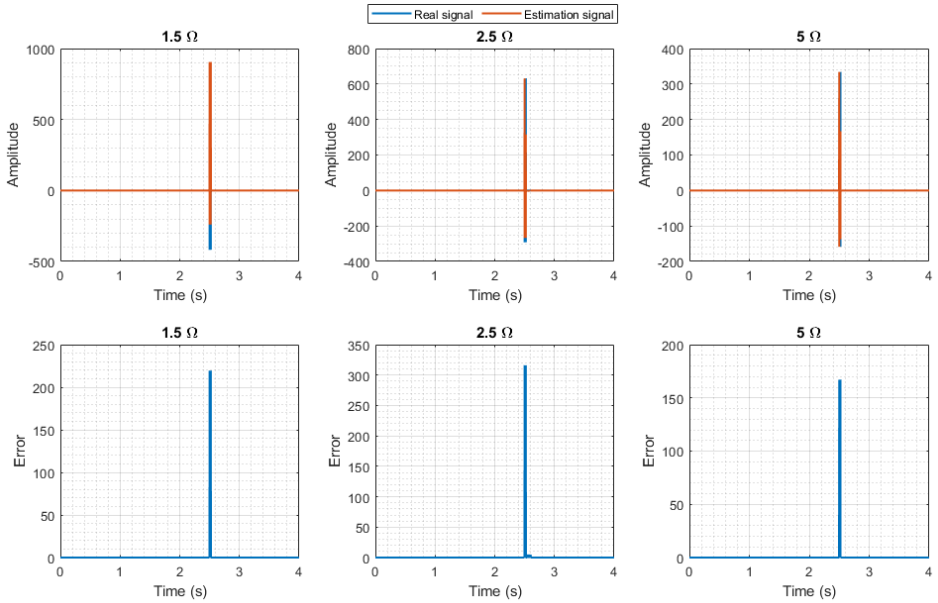

Figure 11. The proposed method performance for the PG fault in the EV.

To asses the performance of the proposed method when a PP fault occurs in EV system, a PP fault is applied on this part of the DC microgrid. According to the simulation results demonstrated in Figure 12, the proposed fault detection method in this paper accurately detects PP fault in the EV system in about 1 ms.

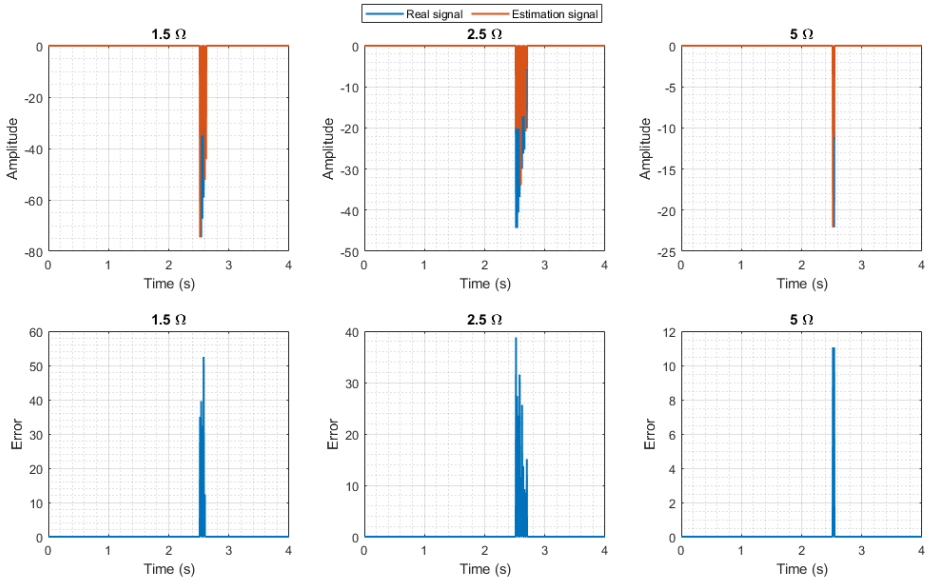

Figure 12. The proposed method performance for the PP fault in the EV.

3.2. Fault Location Results

This section introduces a novel fault location methodology designed for DC microgrids. Simulation results showcase the method's effectiveness in providing swift and accurate fault location across various fault scenarios. The proposed method utilizes a feature matrix for precise estimation by an LSTM model, implemented through MATLAB/Simulink simulations. The fault locator relies on measured voltage and current signals at the IED location, eliminating the need for telecommunication links. Performance evaluation involves applying random faults to the DC microgrid, calculating RMSE, MSE, and MAE; demonstrating the proposed fault location method's excellent performance in fault location. Results and data presented in subsequent sections confirm the method's effectiveness.

3.2.1. Fault Location for Faults with Resistance of 1.5 Ω

To assess the accuracy of the new fault location method for the faults by the resistance of 1.5 Ω, numerous PP and PG faults are applied to the main line of the DC microgrid. The distances, and as a result the line resistances, are selected randomly. Subsequently, as Figure 13 depicts the fault location estimate for different faults applied to the main line. The error value in locating the fault is very low, and the proposed fault location method locates the fault with high accuracy. According to this figure, the value of RMSE is about 5%, and as a result, this method has an accuracy of 95% to locate the faults with the referred fault resistance.

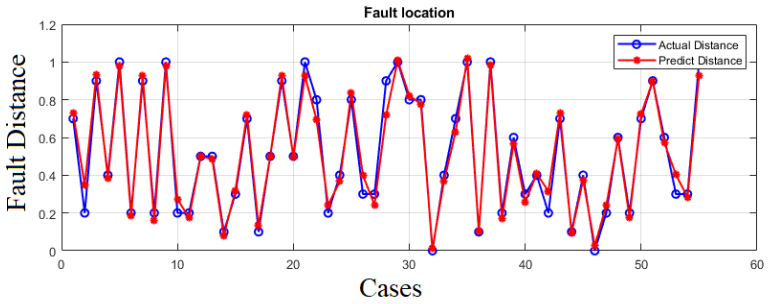

Figure 13. The proposed method accuracy in fault localization for 1.5 Ω.

In Figure 14, we can see the training progress of the LSTM model to locate the fault by a resistance of 1.5 Ω.

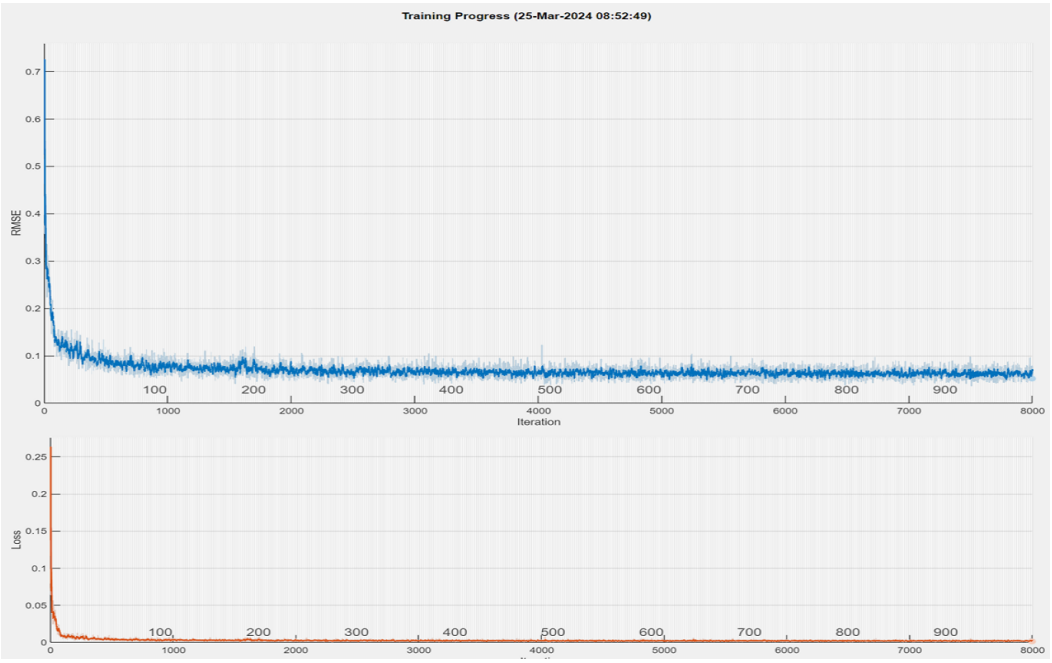

Figure 14. The training progress of LSTM model for 1.5 Ω.

The values for *RMSE*, *MSE*, and *MAE* that present the accuracy of the proposed method are presented in Table 2. According to the achieved values demonstrated in the table, the proposed method has a high accuracy for fault location.

Table 2. Error numerical values in fault location for 1.5 Ω.

	Parameter	Value
1	*RMSE*	0.0522
2	*MSE*	0.0027
3	*MAE*	0.0372

3.2.2. Fault Location for Faults with Resistance of 2.5 Ω

To assess the accuracy of the new fault location method for the faults by fault resistance of 2.5 Ω, similarly, several PP and PG faults are applied to the main line of the DC microgrid. The results for prediction of the fault location when the faults have the resistance of 2.5 Ω are shown in Figure 15. As demonstrated in the figure, the error value, the difference between the actual and predicted value, is still low. Although the error value in this case is bigger by 1 percentage to the 1.5 Ω, the accuracy is still high and is about 93.5%.

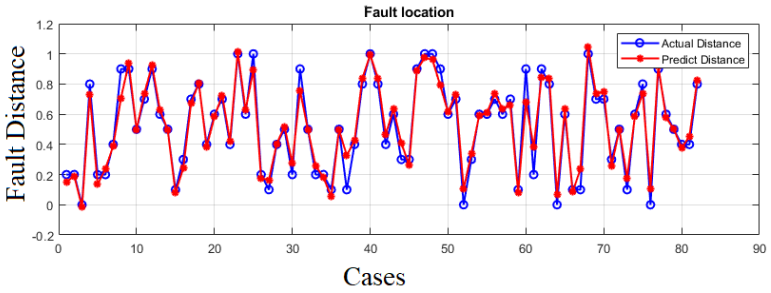

Figure 15. The proposed method accuracy in fault localization for 2.5 Ω.

In Figure 16, the training progress of the LSTM model to locate the fault by a resistance of 2.5 Ω is demonstrated.

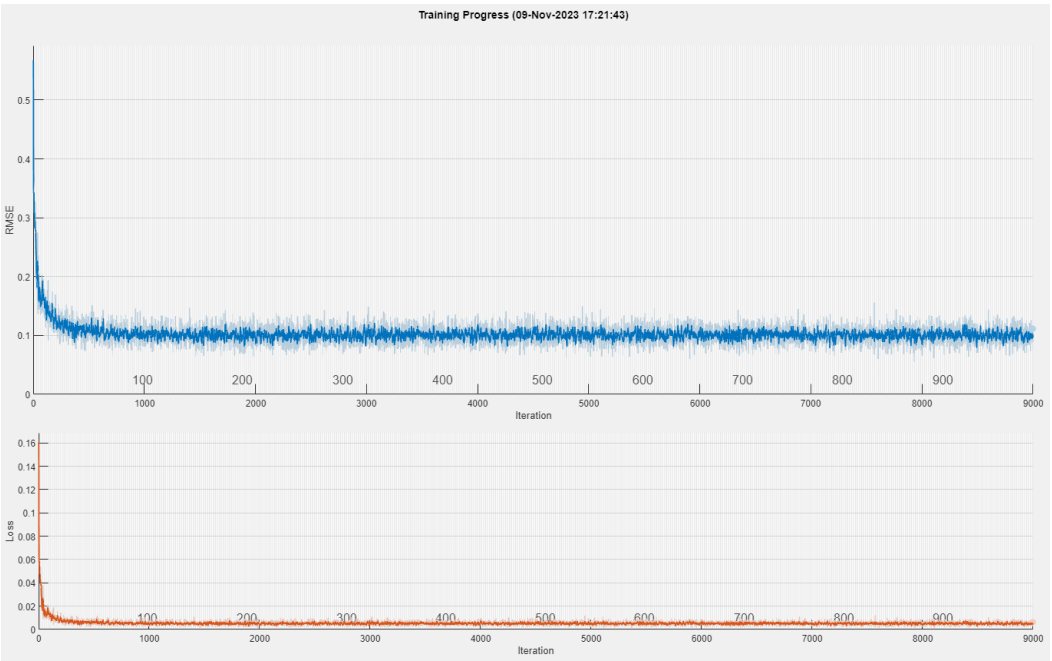

Figure 16. The training progress of LSTM model for 2.5 Ω.

The values for RMSE, MSE, and MAE for fault resistance of 2.5 Ω are also as shown in Table 3. According to this table, there is a notable precision for this fault resistance.

Table 3. Error numerical values in fault location for 2.5 Ω.

	Parameter	Value
1	*RMSE*	0.0665
2	*MSE*	0.0044
3	*MAE*	0.0465

3.2.3. Fault Location for Faults with Resistance of 5 Ω

To assess the fault resistance of 5 Ω, we apply different randomly selected PP and PG faults to the main line of the DC microgrid. By applying different faults the LSTM model provides the prediction results as Figure 17. The results depicted in this figure also validate the high accuracy of the proposed fault location technique.

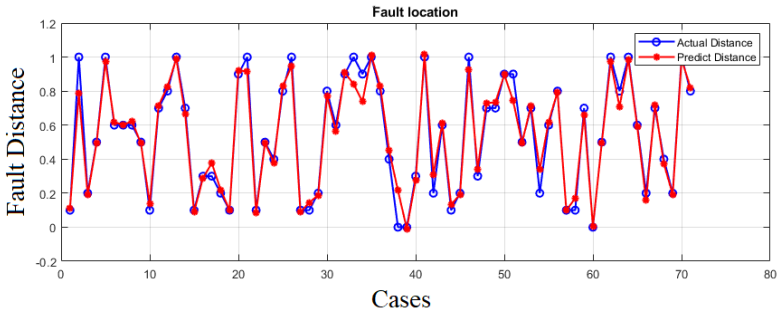

Figure 17. The proposed method accuracy in fault localization for 5 Ω.

In Figure 18, the training progress of the LSTM model to locate the fault by a resistance of 5 Ω is demonstrated.

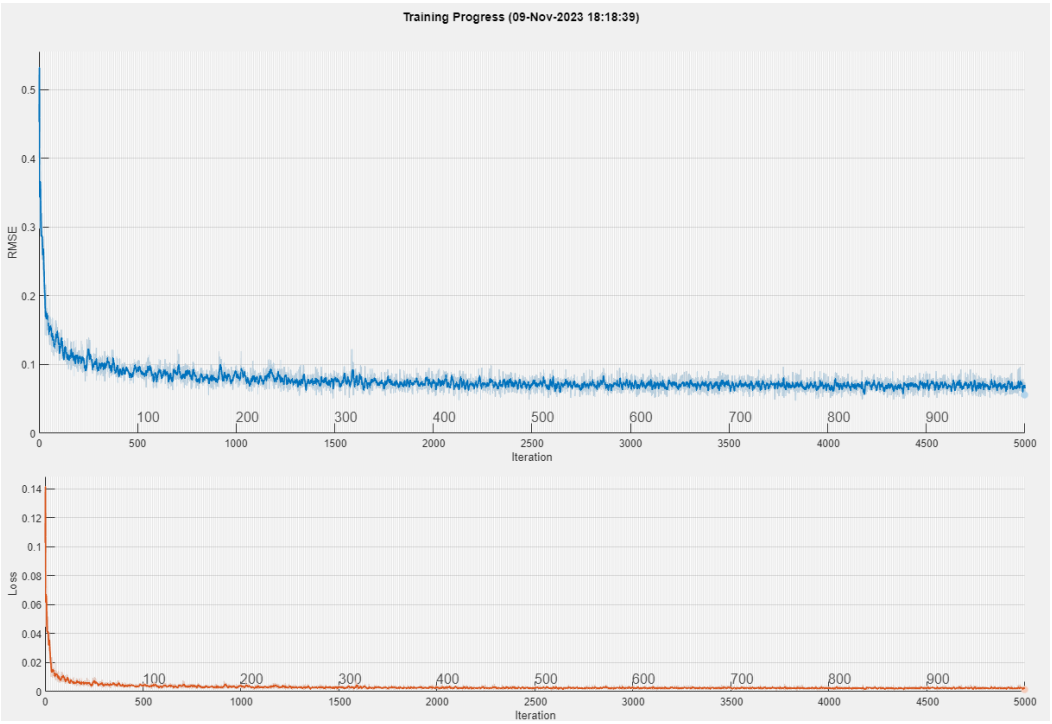

Figure 18. The training progress of LSTM model for 5 Ω.

The values for *RMSE*, *MSE*, and *MAE* for fault resistance of 5 Ω are also shown in Table 4. The *RMSE* value is about 0.0609 for this case, which shows a high precision in predicting the faults location.

Table 4. Error numerical values in fault location for 5 Ω.

	Parameter	Value
1	*RMSE*	0.0609
2	*MSE*	0.0037
3	*MAE*	0.0378

According to the results provided above, the proposed fault location method can estimate the fault location with an accuracy of more than 93%, which is an acceptable range for fault location in a DC microgrid.

4. Comparison of the Proposed Fault Detection Method with Other Existing Methods

In this section, we evaluate the effectiveness of the proposed fault detection method in comparison to several established methodologies in this area. The comparison encompasses key criteria, including speed, computational efficiency, the need for defining thresholds, detection time, etc. Compared to the existing fault detection methods, the proposed method in this paper demonstrates critical advantages. First, it is a swift method of detecting the fault and isolating the DC microgrid components. In addition, this method is threshold-free, which makes it stronger when facing transient states in the DC microgrid. Moreover, compared to the recent studies, the studied DC microgrid encompasses different components, including EV, PV, combined energy storage system, and DC and AC loads.

Table 5 shows the comparison between the protection system proposed in this article and the prior DC microgrid protection methods. Some advantages of the proposed method over prior methods include implementing a combined battery and flywheel hybrid storage systems, and not using telecommunication links. Due to the existence of the flywheel, the battery and flywheel storage system have a fast response to the system changes. These quick changes can mistake the protection systems and cause undesired tripping. In addition, the method presented in this article does not require the use of communication systems. Using protection systems, in addition to increasing the performance speed, also tackles the challenges of telecommunication link uncertainty. Most importantly, the proposed method does not need the threshold consideration that is always a serious challenge for protection systems in DC microgrids.

Table 5. Comparison of the proposed method with other existing methods.

Ref.	Method	SR	Detection Time	ESS	EV/PV	Comm. Links	Threshold
[63]	Pearson correlation coefficient	10 kHz	5 ms	×	PV	×	✓
[64]	Centralized protection	4 kHz	1 ms	Battery	PV	✓	✓
[65]	VMD assisted current	10 kHz	3.95 ms	Fuel cell & Battery	PV	✓	✓
[66]	$H_\infty / H_- / regional$ pole	-	290 ms	×	×	✓	✓
New method	CST & RT	10 kHz	1 ms	Battery and flywheel	EV & PV	×	×

5. Conclusions

To implement the proposed method for fault detection and location in this paper, a DC microgrid is simulated in the MATLAB/Simulink environment. Afterward, the data are taken by sampling the current signal in the main DC bus of the studied network to implement the proposed techniques. The new approach for fault detection harnesses the combined power of compressed sensing (CS) and regression tree (RT). The initial step to implement the proposed method is the sampling of the current signal within various grid

conditions at the Intelligent Electronic Device (IED) location. By simulating a wide range of transient and steady-state scenarios, a comprehensive data set is gathered. Subsequently, CS is employed to process this dataset. Having the imaginary part of the current signal, we undertake an offline procedure to train the RT. Then, having the trained RT, the algorithm checks the estimated and actual value of the signal in an online mode, and if the defined condition is met, the fault will be detected by the proposed algorithm. Afterward, this paper provides an accurate fault location method based on the feature matrix and LSTM model. The process begins with applying numerous faults (PP and PG) along the main DC line. These faults are positioned at various distances in the main DC line, with different fault resistances. Voltages and currents are measured at the time of fault occurrence, and the data are generated. Feature matrices are then calculated, serving as inputs for training of the LSTM model to accurately locate the faults. As the results demonstrate, the proposed method has a high accuracy in fault location.

Author Contributions: Conceptualization, S.S., S.M.M. and M.B.; Methodology, S.S., S.M.M. and M.B.; Software, S.S.; Validation, S.M.M. and M.B.; Formal analysis, S.S.; Resources, S.M.M. and M.B.; Data curation, S.S.; Writing—original draft, S.S. and S.M.M.; Writing—review & editing, S.S., S.M.M. and M.B.; Visualization, S.S. and S.M.M.; Supervision, S.M.M. and M.B.; Project administration, S.M.M. and M.B.; Funding acquisition, S.M.M. All authors have read and agreed to the published version of the manuscript.

Funding: This research received no external funding.

Institutional Review Board Statement: Not applicable.

Informed Consent Statement: Not applicable.

Data Availability Statement: Data is contained within the article.

Conflicts of Interest: The authors declare no conflicts of interest.

Appendix A

Figure A1 depicts the RT for the proposed fault detection method.

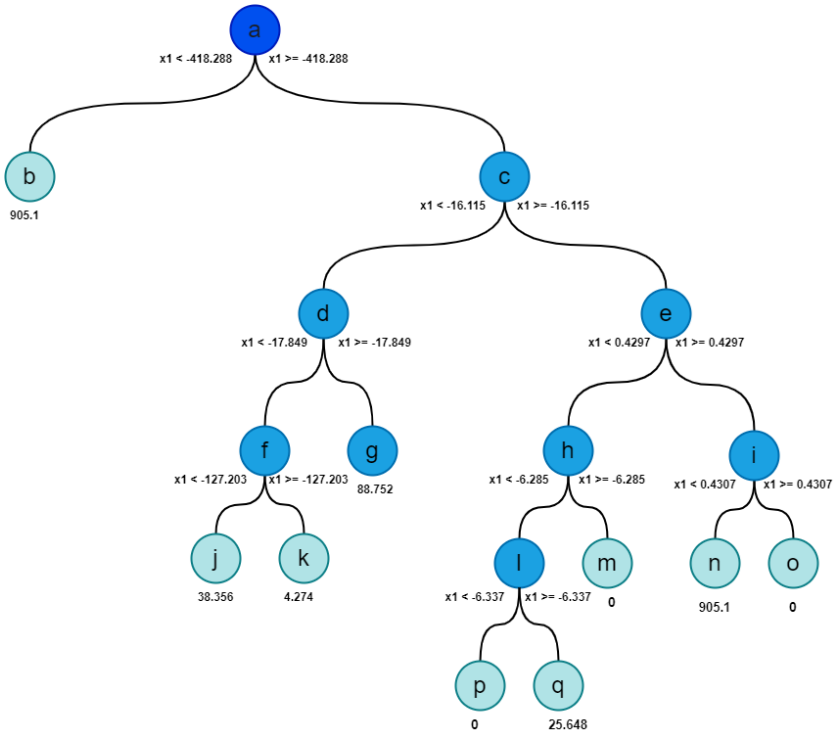

Figure A1. Trained RT in this paper.

References

1. Brenna, M.; Foiadelli, F.; Longo, M.; Zaninelli, D. E-Mobility forecast for the transnational e-corridor planning. *IEEE Trans. Intell. Transp. Syst.* **2015**, *17*, 680–689. [CrossRef]
2. Dhar, S.; Patnaik, R.K.; Dash, P. Fault detection and location of photovoltaic based DC microgrid using differential protection strategy. *IEEE Trans. Smart Grid* **2017**, *9*, 4303–4312. [CrossRef]
3. Chandra, A.; Singh, G.K.; Pant, V. Protection techniques for DC microgrid-A review. *Electr. Power Syst. Res.* **2020**, *187*, 106439. [CrossRef]
4. Justo, J.J.; Mwasilu, F.; Lee, J.; Jung, J.W. AC-microgrids versus DC-microgrids with distributed energy resources: A review. *Renew. Sustain. Energy Rev.* **2013**, *24*, 387–405. [CrossRef]
5. Park, J.D.; Candelaria, J.; Ma, L.; Dunn, K. DC ring-bus microgrid fault protection and identification of fault location. *IEEE Trans. Power Deliv.* **2013**, *28*, 2574–2584. [CrossRef]
6. Shenai, K.; Shah, K. Smart DC micro-grid for efficient utilization of distributed renewable energy. In Proceedings of the IEEE 2011 EnergyTech, Cleveland, OH, USA, 25–26 May 2011; pp. 1–6.
7. Dragičević, T.; Lu, X.; Vasquez, J.C.; Guerrero, J.M. DC microgrids—Part II: A review of power architectures, applications, and standardization issues. *IEEE Trans. Power Electron.* **2015**, *31*, 3528–3549. [CrossRef]
8. Hosseini, S.A.; Abyaneh, H.A.; Sadeghi, S.H.H.; Razavi, F.; Nasiri, A. An overview of microgrid protection methods and the factors involved. *Renew. Sustain. Energy Rev.* **2016**, *64*, 174–186. [CrossRef]
9. Beheshtaein, S.; Cuzner, R.M.; Forouzesh, M.; Savaghebi, M.; Guerrero, J.M. DC microgrid protection: A comprehensive review. *IEEE J. Emerg. Sel. Top. Power Electron.* **2019**. [CrossRef]
10. Marroqui, D.; Blanes, J.M.; Garrigos, A.; Gutierrez, R. Self-powered 380 V DC SiC solid-state circuit breaker and fault current limiter. *IEEE Trans. Power Electron.* **2019**, *34*, 9600–9608. [CrossRef]
11. Mohanty, R.; Pradhan, A.K. Protection of smart DC microgrid with ring configuration using parameter estimation approach. *IEEE Trans. Smart Grid* **2017**, *9*, 6328–6337. [CrossRef]
12. Jayamaha, D.; Lidula, N.; Rajapakse, A. Protection and grounding methods in DC microgrids: Comprehensive review and analysis. *Renew. Sustain. Energy Rev.* **2020**, *120*, 109631. [CrossRef]
13. Shabani, A.; Mazlumi, K. Evaluation of a communication-assisted overcurrent protection scheme for photovoltaic-based DC microgrid. *IEEE Trans. Smart Grid* **2019**, *11*, 429–439. [CrossRef]
14. Amamra, S.A.; Ahmed, H.; El-Sehiemy, R.A. Firefly algorithm optimized robust protection scheme for DC microgrid. *Electr. Power Compon. Syst.* **2017**, *45*, 1141–1151. [CrossRef]
15. Kim, S.; Dujic, D.; Kim, S.N. Protection schemes in low-voltage DC shipboard power systems. In Proceedings of the PCIM Europe 2018; International Exhibition and Conference for Power Electronics, Intelligent Motion, Renewable Energy and Energy Management, Nuremberg, Germany, 5–7 June 2018; pp. 1–7.
16. Javed, W.; Chen, D.; Farrag, M.E.; Xu, Y. System configuration, fault detection, location, isolation and restoration: A review on LVDC microgrid protections. *Energies* **2019**, *12*, 1001. [CrossRef]
17. Farhadi, M.; Mohammed, O.A. A new protection scheme for multi-bus DC power systems using an event classification approach. *IEEE Trans. Ind. Appl.* **2016**, *52*, 2834–2842. [CrossRef]
18. Srivastava, C.; Tripathy, M.; Wang, L. Fault Detection and Classification of DC Microgrid Utilizing Differential Protection Scheme. In Proceedings of the 2022 IEEE IAS Global Conference on Emerging Technologies (GlobConET), Arad, Romania, 20–22 May 2022; pp. 96–101.
19. Dhar, S.; Dash, P.K. Differential current-based fault protection with adaptive threshold for multiple PV-based DC microgrid. *IET Renew. Power Gener.* **2017**, *11*, 778–790. [CrossRef]
20. Hosseini, S.A.; Taheri, B.; Sadeghi, S.H.H.; Nasiri, A. An Overview of DC Microgrid Protection Schemes and the Factors Involved. *Electr. Power Compon. Syst.* **2023**, 1–31.. [CrossRef]
21. Brenna, M.; Foiadelli, F.; Longo, M. Fault detection HVDC systems applied to renewable sources. In Proceedings of the 2016 17th International Conference on Harmonics and Quality of Power (ICHQP), Belo Horizonte, Brazil, 6–19 October 2016; pp. 691–696.
22. Jayamaha, D.; Lidula, N.; Rajapakse, A.D. Wavelet-multi resolution analysis based ANN architecture for fault detection and localization in DC microgrids. *IEEE Access* **2019**, *7*, 145371–145384. [CrossRef]
23. Montoya, R.; Poudel, B.P.; Bidram, A.; Reno, M.J. DC microgrid fault detection using multiresolution analysis of traveling waves. *Int. J. Electr. Power Energy Syst.* **2022**, *135*, 107590. [CrossRef]
24. Sharma, S.; Tripathy, M. Differential Reactor Voltage Based Fault Detection and Classification for Smart DC Microgrid. *IEEE Trans. Ind. Inform.* **2023**, *19*, 11730–11741. [CrossRef]
25. Mohanty, R.; Pradhan, A.K. DC ring bus microgrid protection using the oscillation frequency and transient power. *IEEE Syst. J.* **2018**, *13*, 875–884. [CrossRef]
26. Emhemed, A.A.; Fong, K.; Fletcher, S.; Burt, G.M. Validation of fast and selective protection scheme for an LVDC distribution network. *IEEE Trans. Power Deliv.* **2016**, *32*, 1432–1440. [CrossRef]
27. Mohanty, R.; Balaji, U.S.M.; Pradhan, A.K. An accurate noniterative fault-location technique for low-voltage DC microgrid. *IEEE Trans. Power Deliv.* **2015**, *31*, 475–481. [CrossRef]
28. Yang, X.P.; Feng, T.H.; Zhao, N.B. Fault Transient Analysis of Flexible Medium Voltage DC Distribution. In Proceedings of the 2nd International Conference on Electrical and Electronic Engineering (EEE 2019), Hangzhou, China, 26–27 May 2019; pp. 85–89.

29. Dashti, R.; Daisy, M.; Mirshekali, H.; Shaker, H.R.; Aliabadi, M.H. A survey of fault prediction and location methods in electrical energy distribution networks. *Measurement* **2021**, *184*, 109947. [CrossRef]
30. Dashti, R.; Tahavori, M.; Daisy, M.; Shaker, H.R. A new matching algorithm for fault section estimation in power distribution networks. In Proceedings of the 2018 International Symposium on Advanced Electrical and Communication Technologies (ISAECT), Rabat, Morocco, 21–23 November 2018; pp. 1–4.
31. Zhang, S.; Wang, Y.; Liu, M.; Bao, Z. Data-based line trip fault prediction in power systems using LSTM networks and SVM. *IEEE Access* **2017**, *6*, 7675–7686. [CrossRef]
32. Skydt, M.R.; Bang, M.; Shaker, H.R. A probabilistic sequence classification approach for early fault prediction in distribution grids using long short-term memory neural networks. *Measurement* **2021**, *170*, 108691. [CrossRef]
33. Haque, M.; Shaheed, M.N.; Choi, S. Deep learning based micro-grid fault detection and classification in future smart vehicle. In Proceedings of the 2018 IEEE Transportation Electrification Conference and Expo (ITEC), Long Beach, CA, USA, 13–15 June 2018; pp. 1082–1107.
34. Sharif, A.A.; Karegar, H.K.; Esmaeilbeigi, S. Fault detection and location in dc microgrids by recurrent neural networks and decision tree classifier. In Proceedings of the 2020 10th Smart Grid Conference (SGC), Kashan, Iran, 16–17 December 2020; pp. 1–6.
35. Kar, S.; Samantaray, S.; Zadeh, M.D. Data-mining model based intelligent differential microgrid protection scheme. *IEEE Syst. J.* **2015**, *11*, 1161–1169. [CrossRef]
36. Mishra, D.P.; Samantaray, S.R.; Joos, G. A combined wavelet and data-mining based intelligent protection scheme for microgrid. *IEEE Trans. Smart Grid* **2015**, *7*, 2295–2304. [CrossRef]
37. Mishra, M.; Rout, P.K. Detection and classification of micro-grid faults based on HHT and machine learning techniques. *IET Gener. Transm. Distrib.* **2018**, *12*, 388–397. [CrossRef]
38. Miraftabzadeh, S.M.; Longo, M.; Foiadelli, F.; Bracco, S. Anomaly Detection in Photovoltaic Systems via Deep Learning Autoencoder. In Proceedings of the 2023 International Conference on Smart Energy Systems and Technologies (SEST), Mugla, Turkiye, 4–6 September 2023; pp. 1–6.
39. Manohar, M.; Koley, E.; Ghosh, S. Microgrid protection under wind speed intermittency using extreme learning machine. *Comput. Electr. Eng.* **2018**, *72*, 369–382. [CrossRef]
40. Abdelgayed, T.S.; Morsi, W.G.; Sidhu, T.S. Fault detection and classification based on co-training of semisupervised machine learning. *IEEE Trans. Ind. Electron.* **2017**, *65*, 1595–1605. [CrossRef]
41. James, J.; Hou, Y.; Lam, A.Y.; Li, V.O. Intelligent fault detection scheme for microgrids with wavelet-based deep neural networks. *IEEE Trans. Smart Grid* **2017**, *10*, 1694–1703.
42. Telford, R.D.; Galloway, S.; Stephen, B.; Elders, I. Diagnosis of series DC arc faults—A machine learning approach. *IEEE Trans. Ind. Inform.* **2016**, *13*, 1598–1609. [CrossRef]
43. Wang, Z.; Balog, R.S. Arc fault and flash detection in photovoltaic systems using wavelet transform and support vector machines. In Proceedings of the 2016 IEEE 43rd Photovoltaic Specialists Conference (PVSC), Portland, OR, USA, 5–10 June 2016; pp. 3275–3280.
44. Roy, S.; Nayar, S.; Kumar, S.; Alam, A.; Ghose, T. Bidirectional power flow in dc microgrid and its islanding detection using support vector machine. In Proceedings of the 2019 International Conference on Intelligent Computing and Control Systems (ICCS), Madurai, India, 15–17 May 2019; pp. 42–47.
45. Li, M.; Zhang, H.; Ji, T.; Wu, Q. Fault identification in power network based on deep reinforcement learning. *CSEE J. Power Energy Syst.* **2021**, *8*, 721–731.
46. Liu, Y.; Zhang, S.; Li, L.; Wang, S.; Lu, T.; Yu, H.; Liu, W. A machine learning-based fault identification method for microgrids with distributed generations. *J. Phys. Conf. Ser.* **2022**, *2360*, 012019. [CrossRef]
47. Miraftabzadeh, S.M.; Foiadelli, F.; Longo, M.; Pasetti, M. A survey of machine learning applications for power system analytics. In Proceedings of the 2019 IEEE International Conference on Environment and Electrical Engineering and 2019 IEEE Industrial and Commercial Power Systems Europe (EEEIC/I&CPS Europe), Genoa, Italy, 11–14 June 2019; pp. 1–5.
48. Duarte, M.F.; Eldar, Y.C. Structured compressed sensing: From theory to applications. *IEEE Trans. Signal Process.* **2011**, *9*, 4053–4085. [CrossRef]
49. Loh, W.Y. Classification and regression trees. *Wiley Interdiscip. Rev. Data Min. Knowl. Discov.* **2011**, *1*, 14–23. [CrossRef]
50. Shen, L.; Cheng, Q.; Cheng, Y.; Wei, L.; Wang, Y. Hierarchical control of DC micro-grid for photovoltaic EV charging station based on flywheel and battery energy storage system. *Electr. Power Syst. Res.* **2020**, *179*, 106079. [CrossRef]
51. Sistani, A.; Hosseini, S.A.; Sadeghi, V.S.; Taheri, B. Fault Detection in a Single-Bus DC Microgrid Connected to EV/PV Systems and Hybrid Energy Storage Using the DMD-IF Method. *Sustainability* **2023**, *15*, 16269. [CrossRef]
52. Candès, E.J.; Romberg, J.; Tao, T. Robust uncertainty principles: Exact signal reconstruction from highly incomplete frequency information. *IEEE Trans. Inf. Theory* **2006**, *52*, 489–509. [CrossRef]
53. Donoho, D.L. Compressed sensing. *IEEE Trans. Inf. Theory* **2006**, *52*, 1289–1306. [CrossRef]
54. Grcić, I.; Pandžić, H.; Novosel, D. Fault detection in dc microgrids using short-time fourier transform. *Energies* **2021**, *14*, 277. [CrossRef]
55. Miraftabzadeh, S.M.; Colombo, C.G.; Longo, M.; Foiadelli, F. K-Means and Alternative Clustering Methods in Modern Power Systems. *IEEE Access* **2023**, *11*, 119596–119633. [CrossRef]
56. Cover, T.; Hart, P. Nearest neighbor pattern classification. *IEEE Trans. Inf. Theory* **1967**, *13*, 21–27. [CrossRef]

57. Morgan, J.N.; Sonquist, J.A. Problems in the analysis of survey data, and a proposal. *J. Am. Stat. Assoc.* **1963**, *58*, 415–434. [CrossRef]
58. Yang, J.; Stenzel, J. Short-term load forecasting with increment regression tree. *Electr. Power Syst. Res.* **2006**, *76*, 880–888. [CrossRef]
59. Taheri, B.; Sedighizadeh, M.; Nasiri, M.R.; Sheikhi Fini, A. Proposing a Novel Approach Non-Intrusive Load Monitoring Based on Feature Extraction Matrix and KNN Machine Learning Model. *Technovations Electr. Eng. Green Energy Syst.* **2024**, *2*, 108–127.
60. Taheri, B.; Salehimehr, S.; Sedighizadeh, M. A fault-location algorithm for parallel line based on the long short-term memory model using the distributed parameter line model. *Int. Trans. Electr. Energy Syst.* **2021**, *31*, e13032. [CrossRef]
61. Bareth, R.; Yadav, A.; Gupta, S.; Pazoki, M. Daily average load demand forecasting using LSTM model based on historical load trends. *IET Gener. Transm. Distrib.* **2024**, *18*, 952–962. [CrossRef]
62. Moradzadeh, A.; Zakeri, S.; Shoaran, M.; Mohammadi-Ivatloo, B.; Mohammadi, F. Short-term load forecasting of microgrid via hybrid support vector regression and long short-term memory algorithms. *Sustainability* **2020**, *12*, 7076. [CrossRef]
63. Kong, L.; Nian, H. Fault detection and location method for mesh-type DC microgrid using pearson correlation coefficient. *IEEE Trans. Power Deliv.* **2020**, *36*, 1428–1439. [CrossRef]
64. Mohanty, R.; Sahoo, S.; Pradhan, A.K.; Blaabjerg, F. A cosine similarity-based centralized protection scheme for DC microgrids. *IEEE J. Emerg. Sel. Top. Power Electron.* **2021**, *9*, 5646–5656. [CrossRef]
65. Sharma, N.K.; Samantaray, S.R.; Bhende, C.N. VMD-enabled current-based fast fault detection scheme for DC microgrid. *IEEE Syst. J.* **2021**, *16*, 933–944. [CrossRef]
66. Mola, M.; Afshar, A.; Meskin, N.; Karrari, M. Distributed fast fault detection in DC microgrids. *IEEE Syst. J.* **2020**, *16*, 440–451. [CrossRef]